

Cite this: *Dalton Trans.*, 2015, **44**, 19820

## Tin(II) ketoacidoximates: synthesis, X-ray structures and processing to tin(II) oxide†‡

Jayaprakash Khanderi, Bambar Davaasuren, Buthainah Ameen Alshankiti and Alexander Rothenberger\*

Tin(II) ketoacidoximates of the type  $[\text{HON}=\text{CRCOO}]_2\text{Sn}$  ( $\text{R} = \text{Me}$  **1**,  $\text{CH}_2\text{Ph}$  **2**) and  $(\text{MeON}=\text{CMeCOO})_3\text{Sn}]^- \text{NH}_4^+ \cdot 2\text{H}_2\text{O}$  **3** were synthesized by reacting pyruvate- and hydroxyl- or methoxylamine  $\text{RONH}_2$  ( $\text{R} = \text{H}, \text{Me}$ ) with tin(II) chloride dihydrate  $\text{SnCl}_2 \cdot 2\text{H}_2\text{O}$ . The single crystal X-ray structure reveals that the geometry at the Sn atom is trigonal bipyramidal in **1**, **2** and trigonal pyramidal in **3**. Inter- or intramolecular hydrogen bonding is observed in **1–3**. Thermogravimetric (TG) analysis shows that the decomposition of **1–3** to SnO occurs at ca. 160 °C. The evolved gas analysis during TG indicates complete loss of the oximate ligand in one step for **1** whereas a small organic residue is additionally removed at temperatures >400 °C for **2**. Above 140 °C,  $[\text{HON}=\text{C}(\text{Me})\text{COO}]_2\text{Sn}$  (**1**) decomposes in air to spherical SnO particles of size 10–500 nm. Spin coating of **1** on Si or a glass substrate followed by heating at 200 °C results in a uniform film of SnO. The band gap of the produced SnO film and nanomaterial was determined by diffuse reflectance spectroscopy to be in the range of 3.0–3.3 eV. X-ray photoelectron spectroscopy indicates surface oxidation of the SnO film to  $\text{SnO}_2$  in ambient atmosphere.

Received 11th August 2015,  
Accepted 21st October 2015

DOI: 10.1039/c5dt03103f

www.rsc.org/dalton

## Introduction

Semiconducting stannic oxide ( $\text{SnO}_2$ ) and stannous oxide (SnO) have attracted considerable research interest in the area of electronics and optoelectronics.  $\text{SnO}_2$  has found application in transparent conducting electrodes as indium tin oxide (ITO),<sup>1,2</sup> thin film transistors,<sup>3,4</sup> sensors,<sup>5,6</sup> heat reflecting filters<sup>7</sup> and solar cells.<sup>7</sup> Research on SnO is focused on the synthesis of nanostructures<sup>8–12</sup> as anode materials in rechargeable Li ion batteries.<sup>13,14</sup> Tin(II) oxide is also a versatile intermediate to metallic tin,<sup>15</sup>  $\text{Sn}_3\text{O}_4$ <sup>16,17</sup> and  $\text{SnO}_2$ .<sup>18</sup> SnO thin films have shown a hole mobility of  $2.4 \text{ cm}^2 \text{ V}^{-1} \text{ s}^{-1}$ , the largest among the p-type oxide semiconductors.<sup>19</sup> Antimony doped SnO shows n-type conduction,<sup>20</sup> opening the possibility of bipolar oxide TFTs.<sup>21</sup> Homo-junction p–n diodes with p-type SnO and n-type  $\text{SnO}_2$ <sup>22</sup> thin film transistors and inverters have

been investigated.<sup>19,23–27</sup> The recent literature reports a variety of physical methods such as e-beam evaporation, reactive/radio-frequency/magnetron sputtering and pulsed laser deposition to deposit p-type SnO thin films.<sup>28–30</sup> Chemical methods involve vapor phase deposition using molecular precursors such as  $\text{Sn}_6\text{O}_4(\text{OSiMe}_3)_4$ ,  $[\{\text{Sn}(\text{OSiMe}_3)_2\}_2]$ ,<sup>31</sup> Sn(II)bis(ureide) (ureide =  ${}^t\text{BuNCONMe}_2$ ),<sup>32</sup> bis(1-dimethylamino-2-methyl-2-propoxy)tin,<sup>33</sup>  $[\text{Sn}(\mu\text{-ONep})_2]_\infty$  (ONep =  $\text{OCH}_2\text{CMe}_3$ )<sup>34</sup> and solution based methods using  $\text{SnCl}_2 \cdot 2\text{H}_2\text{O}$  and  $\text{NH}_3(\text{aq.})$ .<sup>35</sup> The formation of elemental tin in SnO films<sup>31,34</sup> and sub-stoichiometric tin oxide<sup>34</sup> at higher deposition temperatures (>300 °C) is the drawback of reported routes.<sup>31,34,35</sup> The challenge in the preparation of SnO films is to find a low-temperature route to crystalline SnO, avoiding disproportionation or oxidation to  $\text{SnO}_2$  and the scale-up of optimized SnO film deposition.<sup>19,22,32,36,37</sup>

Metal complexes with oxime/oximate ligands have been extensively studied and reviewed.<sup>38,39</sup> One important aspect of oximate ligands, derived from the reaction of pyruvic or glyoxylic acid with hydroxylamines, is the complete decomposition to  $\text{H}_2\text{O}$ ,  $\text{CO}_2$ ,  $\text{CH}_3\text{CN}$  and functionalized nitriles below 200 °C.<sup>40,41</sup> Thus, it is of interest to examine oximate complexes of tin(II) that could address the challenges associated with SnO formation at lower temperatures.

Cyanoximate and ketoacidoximate complexes of Sn(IV) have been reported.<sup>42,43</sup> The Sn(IV) in cyanoximate complexes, which also show cytotoxicity, are mononuclear and tetranuclear with a trigonal pyramidal geometry,<sup>42</sup> whereas Sn(IV)

Physical Sciences and Engineering Division, 4700 King Abdullah University of Science & Technology (KAUST), Thuwal, 23955-6900, Kingdom of Saudi Arabia.

E-mail: alexander.rothenberger@kaust.edu.sa; Fax: +966 12 8021258;

Tel: +966 12 808 0745

† In memory of Professor Ken Wade.

‡ Electronic supplementary information (ESI) available: IR, gas phase IR, mass of decomposition products, and UV-Vis spectrum of SnO thin films. Details of atomic coordinates, anisotropic atomic displacement parameters, bond lengths and angles for the reported complexes, XRD and SEM of decomposition product of **2**, XPS, and  $I$ - $V$  characteristics of the film. CCDC 1048727–1048729. For ESI and crystallographic data in CIF or other electronic format see DOI: 10.1039/c5dt03103f

ketoacidoximates are reported to be monomeric with Sn(IV) in octahedral and trigonal bipyramidal geometries.<sup>43</sup> The other reported complexes contain ketoacidoximate ligands with Pd, Ru, Rh, Ir,<sup>44,45</sup> Mn,<sup>46</sup> Ti,<sup>47</sup> Ni,<sup>48</sup> Cu,<sup>49,50</sup> Co,<sup>44,51,52</sup> Zn,<sup>53</sup> Cd,<sup>50</sup> alkali,<sup>54</sup> and alkaline earth<sup>55</sup> metal ions. The interest in these complexes was due to the fact that: (1) they act as an intermediate in the metal activated synthesis of  $\alpha$ -amino acids,<sup>45</sup> (2) the oximate ligands are structurally analogous to 2-amino acids and the complexes have shown medical and biological functions<sup>46,52,56</sup> and (3) they are used in the synthesis of metal<sup>57</sup> and metal oxide<sup>57–61</sup> nanoparticles and thin films.

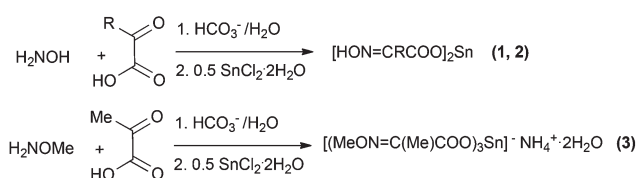
Here, we report the synthesis and crystal structures of tin(II) ketoacidoximate complexes **1–3**, experimental conditions for the synthesis and detailed characterization of SnO nanoparticles and thin films obtained by the decomposition of **1** and **2**.

## Results and discussion

Tin(II) ketoacidoximate complexes **1–3** were synthesized by the condensation reaction of  $\alpha$ -ketocarboxylate and hydroxyl- or methoxyl amine with tin(II) chloride dihydrate in water (Scheme 1). **1** and **2** are isolated as crystalline solids in good yield (67–78%) whereas **3** was isolated in poor yield (~10%). All the complexes are soluble in *N,N*-dimethyl formamide and dimethyl sulfoxide and sparingly soluble in methanol and ethanol. The IR spectra of **1–3** show characteristic absorptions between 1650 and 550  $\text{cm}^{-1}$  (ESI Fig. S1†). The absorption bands at 1620  $\text{cm}^{-1}$  (C=N), 1590  $\text{cm}^{-1}$  (asymmetric vibrations of  $\text{COO}^-$ ),<sup>51</sup> 1350  $\text{cm}^{-1}$  ( $\text{-C=O}$  symmetric or  $\text{CH}_3$ ), 1050  $\text{cm}^{-1}$  (N–O), and 850  $\text{cm}^{-1}$  ( $\text{-OCO-}$  in plane)<sup>43</sup> could be assigned unambiguously. The appearance of  $\nu(\text{sym})$  and  $\nu(\text{asym})$  COO bands indicates possible  $\pi$ -delocalization of the C–O bond. The absorption bands at 3280–3290  $\text{cm}^{-1}$  for **3** could be assigned to NH stretching vibrations of the ammonium ion. The NMR chemical shifts observed for **1**, **2** and **3** are in agreement with the previously reported transition metal complexes.<sup>51,53</sup>

### Description of the molecular structures of **1–3**

The crystal structures of **1**, **2** and **3** were determined from single crystal X-ray diffraction data. Fig. 1a–c show the molecular geometry, bonding and atom labelling of **1**, **2** and **3**. The details of data collection and refinement are summarized in Table 1.



**Scheme 1** Synthesis of Sn(II) ketoacidoximates, where R = Me **1**,  $\text{CH}_2\text{Ph}$  **2**.

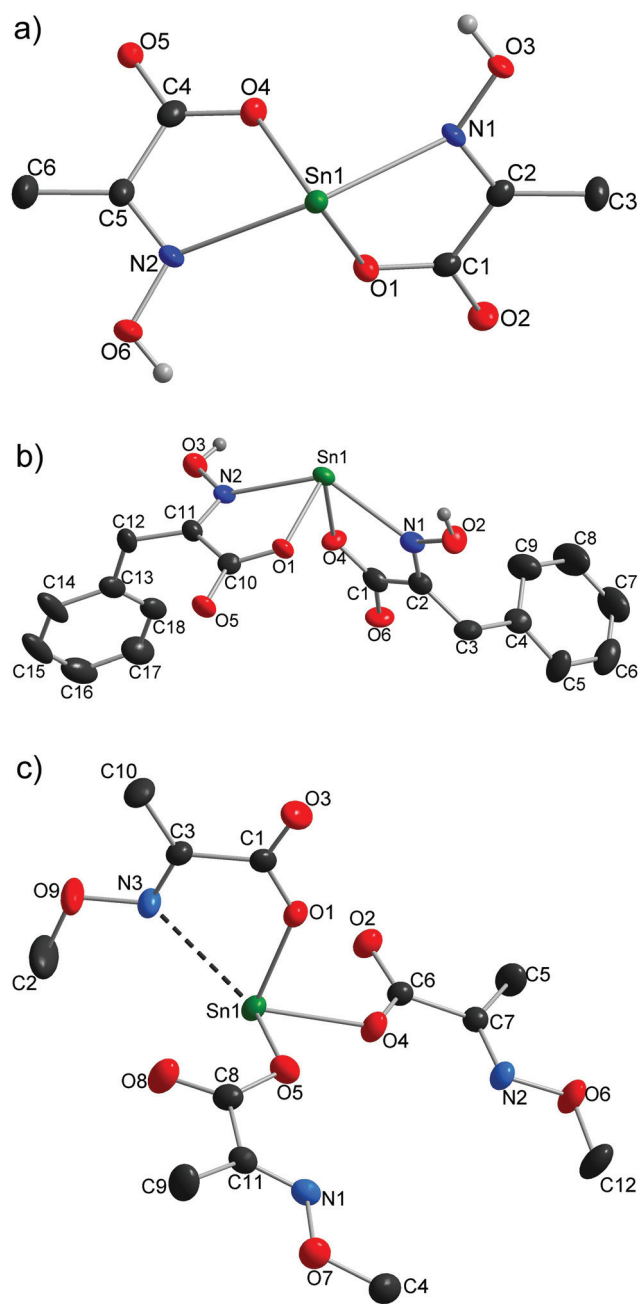


**Fig. 1** Solid state structure of (a) **1**, (b) **2** and (c) anionic part of **3**; H atoms on C, and the solvate molecules of **3** were omitted for clarity; thermal ellipsoids are drawn at the 50% probability level. Selected bond lengths [Å] and angles [°]: **1** Sn(1)–O(1) 2.1776(18), Sn(1)–O(4) 2.2038(18), Sn(1)–N(1) 2.508(2), Sn(1)–N(2) 2.526(2), O(1)–Sn(1)–O(4) 85.90(7), O(1)–Sn(1)–N(1) 67.29(7), O(4)–Sn(1)–N(1) 83.38(8), O(1)–Sn(1)–N(2) 83.17(7), O(4)–Sn(1)–N(2) 66.86(8), N(1)–Sn(1)–N(2) 139.50(8), **2** Sn(1)–O(1) 2.167(5), Sn(1)–O(4) 2.175(6), Sn(1)–N(1) 2.487(8), Sn(1)–N(2) 2.391(8), O(4)–Sn(1)–N(1) 67.7(2), O(1)–Sn(1)–O(4) 86.2(3), N(2)–Sn(1)–N(1) 132.9(3), O(1)–Sn(1)–N(2) 70.0(3), O(4)–Sn(1)–N(2) 74.8(2), O(1)–Sn(1)–N(1) 79.9(3), **3** Sn(1)–O(5) 2.1782(12), Sn(1)–O(1) 2.1792(12), Sn(1)–O(4) 2.1988(12), O(5)–Sn(1)–O(1) 82.45(4), O(5)–Sn(1)–O(4) 77.36(4), O(1)–Sn(1)–O(4) 81.55(4), C(1)–O(1)–Sn(1) 133.15(9), C(6)–O(4)–Sn(1) 113.13(8), C(8)–O(5)–Sn(1) 112.68(10).

**Table 1** Details of the X-ray data collection and refinement for **1**, **2** and **3**

Compound	C <sub>12</sub> H <sub>16</sub> N <sub>4</sub> O <sub>12</sub> Sn <sub>2</sub> ( <b>1</b> )	C <sub>18</sub> H <sub>16</sub> N <sub>2</sub> O <sub>6</sub> Sn ( <b>2</b> )	C <sub>12</sub> H <sub>26</sub> N <sub>4</sub> O <sub>11</sub> Sn ( <b>3</b> )
Formula weight	645.68	475.05	521.06
Crystal system	Triclinic	Orthorhombic	Monoclinic
Space group	<i>P</i> $\bar{1}$	<i>P</i> 2 <sub>1</sub> 2 <sub>1</sub> 2 <sub>1</sub>	<i>C</i> 2/ <i>c</i>
Formula unit, <i>Z</i>	2	4	8
Radiation, $\lambda/\text{\AA}$	Mo K $\alpha$ , 0.71073		
Monochromator	Graphite		
Temperature/K	150(2)		
<i>a</i> / $\text{\AA}$	9.3126(6)	12.039(5)	17.653(4)
<i>b</i> / $\text{\AA}$	11.0220(6)	12.259(5)	14.077(3)
<i>c</i> / $\text{\AA}$	11.5938(6)	12.506(5)	18.854(4)
$\alpha$ / $^\circ$	113.644(4)	90	90
$\beta$ / $^\circ$	108.010(4)	90	117.11(3)
$\gamma$ / $^\circ$	93.80	90	90
<i>V</i> / $\text{\AA}^3$	1011.7(4)	1845.7(13)	4170.6(18)
$\rho_{\text{calc.}}/\text{g cm}^{-3}$	2.120	1.709	1.660
$\mu/\text{mm}^{-1}$	2.538	1.422	1.285
<i>F</i> (000)	624	944	2112
2 $\theta$ max./ $^\circ$	59.32	58.54	58.44
No. ref., <i>I</i> > 2 $\sigma$ ( <i>I</i> )	9854	17 869	10 110
<i>hkl</i> range	-12 < <i>h</i> < 12 -15 < <i>k</i> < 15 -15 < <i>l</i> < 13	-16 < <i>h</i> < 16 -14 < <i>k</i> < 16 -17 < <i>l</i> < 17	-24 < <i>h</i> < 22 -16 < <i>k</i> < 19 -25 < <i>l</i> < 23
Unique ref., parameters	5018, 281	4985, 241	5478, 349
<i>R</i> <sub>int</sub>	0.018	0.129	0.064
<i>R</i> <sub>1</sub> <sup>a</sup>	0.020	0.054	0.047
<i>wR</i> <sub>2</sub> <sup>b</sup>	0.054	0.075	0.118
Goof <sup>c</sup>	1.089	1.072	0.999
Max./min. $\Delta\rho/e \text{\AA}^{-3}$	0.67/-0.52	0.70/-0.75	0.69/-0.71

<sup>a</sup>  $R_1 = \sum(|F_o| - |F_c|)/\sum|F_o|$ . <sup>b</sup>  $wR_2 = \{\sum[w(|F_o|^2 - |F_c|^2)^2]/\sum[w(|F_o|^4)]\}^{1/2}$  and  $w = 1/[\sigma^2(F_o^2) + (nP)^2 + mP]$  where  $P = (F_o^2 + 2F_c^2)/3$ . <sup>c</sup> Goof =  $[\sum_{hkl} w(|F_o| - |F_c|)^2/(n_{\text{data}} - n_{\text{var}})]^{1/2}$ .

The crystal structure of **1** and **2** contains two bidentate 2-oxyiminopropionato anions, which are bonded to the Sn core through the oxime nitrogen atom and one of the carboxylic oxygen atoms forming a *trans* complex with a butterfly configuration (Fig. 1a and b). The Sn(II) atom lies on an inversion centre. A distorted trigonal bipyramidal geometry around the Sn atom is enforced by the stereochemically active lone pair on the tin(II) atom in **1** and **2**, as observed previously<sup>62</sup> and confirmed by a  $\tau$ -test.<sup>63</sup> The Sn–O distances of 2.178(2)–2.204(2) Å in **1**, 2.167(5)–2.175(6) Å in **2** and Sn–N distances 2.508(2)–2.526(2) Å in **1**, 2.487(8)–2.391(8) Å in **2** are similar to those observed in Sn<sub>6</sub>(O)<sub>4</sub>(OSiMe<sub>3</sub>)<sub>4</sub>,<sup>31</sup> [<sup>t</sup>BuNCONMe<sub>2</sub>]<sub>2</sub>Sn<sup>32</sup> as well as Sn(II) complexes containing poly-functional ligands.<sup>64–66</sup> Extensive donor type intermolecular hydrogen bonding exists between –NOH and COO groups in both the molecules.

Short C–O bonding distances of *d*(C1–O1) = 1.272(3) Å and *d*(C1–O2) = 1.240(3) Å (**1**) and *d*(C1–O4) = 1.2774(4) Å and *d*(C1–O6) = 1.2379(5) Å (**2**) in carboxylic groups suggest  $\pi$ -delocalization, which is probably caused by H-bonding and intermolecular Sn←O dative interactions. A similar  $\pi$ -delocalization of the C–O bond is also observed in Co(III), Ni(II) and Zn(II) 2-oxyiminopropionate complexes.<sup>48,51,53</sup> The atomic coordinates, anisotropic atomic displacement parameters, bond lengths and angles are listed in Tables S1–S8 (ESI<sup>†</sup>) respectively.

The first structural difference between **1**, **2** and the previously reported Ni(II), Co(III), Zn(II), Cu(II) and Cd(II) complexes is the long Sn–N bond distance. This bond length ranges between 2.391(2) and 2.526(8) Å for **1** and **2** while it is 2.111(1), 1.875(1), 2.334(2), 2.049(2), and 2.461(15) Å for Ni–N, Co–N, Zn–N, Cu–N, and Cd–N respectively.<sup>48,51,53</sup> The long metal–N bond distance is also observed in the sodium oximate complex.<sup>54</sup> The other interatomic distances in both **1** and **2** are in the same range as that found in the literature.<sup>45,67,68</sup> The second difference is the O–Sn–N bite angle of the ligand to the metal ion. The bite angles in **1** are 67.29 $^\circ$ (7) and 66.86 $^\circ$ (8) and are 70.0 $^\circ$ (8) and 67.7 $^\circ$ (2) in **2**. In the similar Cu(II)<sup>49</sup> complex it is 80.69(6) $^\circ$  and it decreases in Zn(II)<sup>53</sup> to 77.69(1) $^\circ$  and in Cd(II)<sup>50</sup> to 67.88(5) $^\circ$  and 65.77(5) $^\circ$ . The smaller bite angle of the ligand in **1** and **2** as well as in the Cd(II) complex is related to the larger ionic radii of Sn(II) and Cd(II) ions.

The Sn atom, in the crystal structure of **3**, is coordinated by three monodentate 2-methoxyiminopropionato-ligands forming a perfect trigonal bipyramidal geometry with the  $\tau$ -value of unity.<sup>63,69</sup> The three-fold coordination of the Sn(II) ion by COO<sup>−</sup> groups results in the accumulation of negative charge on the Sn atom, which is balanced by NH<sub>4</sub><sup>+</sup> counter ions. The H<sub>2</sub>O molecules form H-bonds with oxygen atoms of the carboxyl groups (ESI Fig. S2<sup>†</sup>). The Sn–O distances *d*(2.178(2)–2.199(1)Å) are in good agreement with the distances reported in the literature.<sup>69</sup> Similar to **1** and **2**, short C–O distances, *d*(C3–O5) = 1.237(6)Å and *d*(C3–O4) = 1.287(6)Å, are found in the carboxylic group of the 2-methoxyiminopropionato-ligands. However, the Sn1...N3 distance is 2.862(1)Å, longest among reported oximate-complexes. The atomic coordinates, interatomic distances and angles are listed in Tables S9–S12 (ESI<sup>†</sup>). The interatomic distances in this structure are close to the distances found in similar tin coordination complexes and tin oxides.<sup>45,67,68</sup>

### Thermal decomposition of **1**, **2** and **3**

Thermal behaviours of **1**–**3** were studied under nitrogen and air atmospheres by thermogravimetry, TG coupled IR and mass spectrometry. Fig. 2a is the TG curve for **1** under N<sub>2</sub>. The decomposition is not affected by the reaction atmosphere (air or nitrogen) and takes place between 155 and 160 °C. The residual mass observed in N<sub>2</sub> (36.9%) and air (43.4%) agrees well with the theoretical value for the formation of SnO (41.5%) for **1**, implying complete decomposition of the ligand. This is supported by the Gram–Schmid curve showing one maximum for the IR signal, indicating simultaneous removal of all gaseous fragments (ESI Fig. S3<sup>†</sup>). The IR spectra and mass spectrometry of the gases evolved during the decomposition of **1** could be assigned to water, CO, CO<sub>2</sub>, and acetonitrile (ESI Fig. S4 and S5<sup>†</sup>). The fragments observed in the TG-MS of **2** are H<sub>2</sub>O, CO, CH<sub>3</sub>CN, CO<sub>2</sub> benzene, toluene and benzyl cyanide (Fig. 2b: only the fragments with higher *m/z* are shown). Decomposition of similar Zn and alkali metal complexes indicates a second order Beckmann rearrangement with elimination of CH<sub>3</sub>CN, H<sub>2</sub>O and CO<sub>2</sub>. The metal complex with a monoalkylcarbonate ligand is suggested as the intermediate,

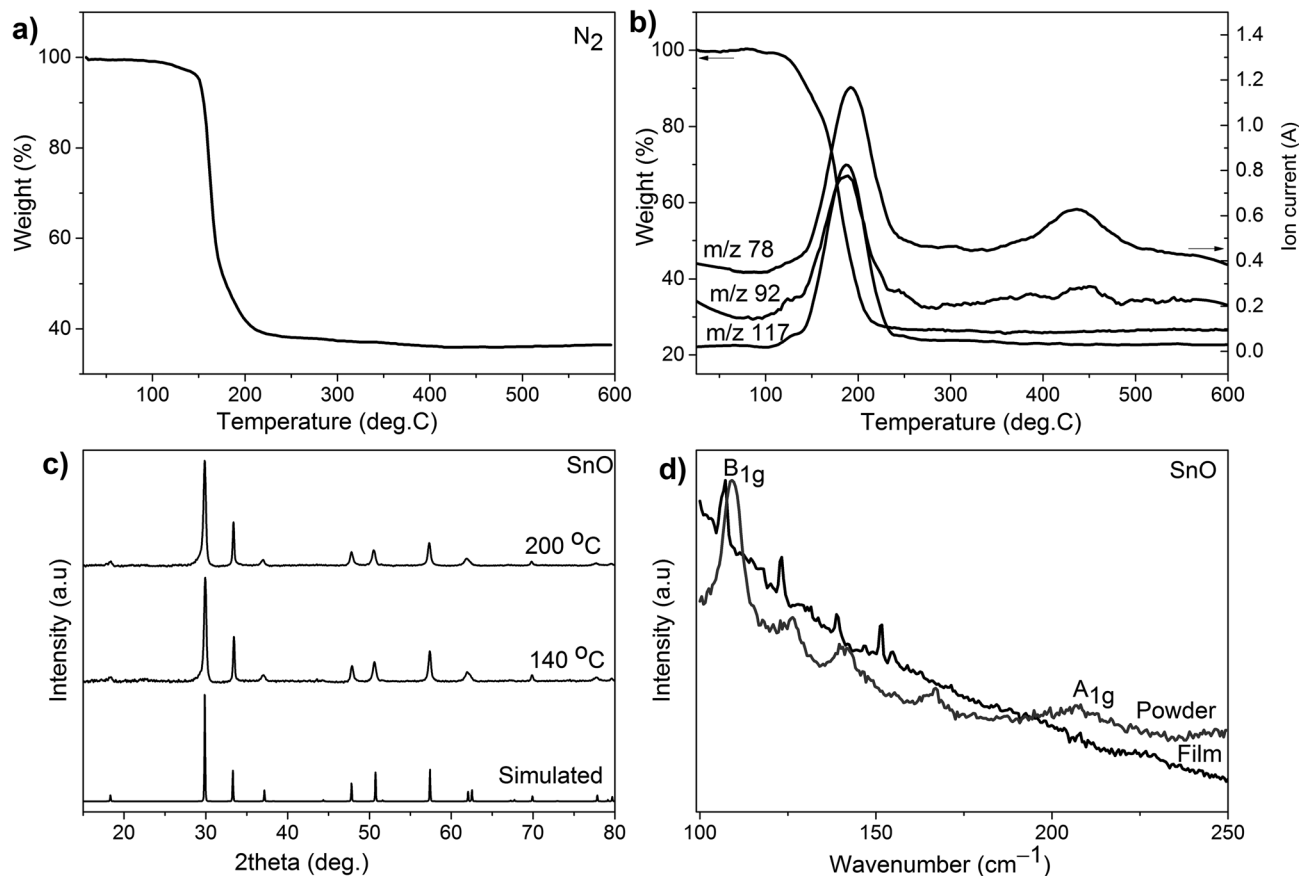


**Fig. 2** (a) The TG for decomposition of bis(2-(hydroxyimino)propionato) tin(II) **1** measured by heating at  $10\text{ }^{\circ}\text{C min}^{-1}$  in a nitrogen flow of  $20\text{ mL min}^{-1}$ . (b) TG and TG-MS of bis[2-(hydroxyimino)3-phenyl-propionato] tin(II) **2** measured by heating at  $5\text{ }^{\circ}\text{C min}^{-1}$  in a helium flow of  $20\text{ mL min}^{-1}$ . The ion current signals are smoothed and normalized. (c) XRD and (d) Raman spectra of SnO powder and films formed by the decomposition of bis(2-(hydroxyimino)propionato) tin(II) **1** at  $200\text{ }^{\circ}\text{C}$ .

which finally forms the metal oxide.<sup>41,54</sup> A similar decomposition pathway could be responsible for the formation of SnO from **1** and **2** (Scheme 2).

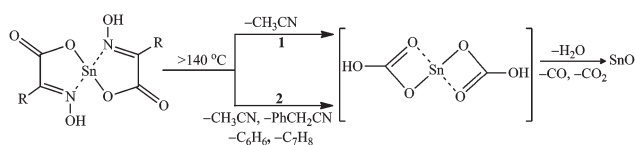
The CHN analysis of the residue obtained after heating of **1** in air shows the average carbon of 1.65% for decomposition temperatures between 140 and  $180\text{ }^{\circ}\text{C}$  whereas a carbon value of 0.86% for the temperature of  $200\text{ }^{\circ}\text{C}$  (ESI, Table 13<sup>†</sup>). Carbon contents of <1% have been reported for ZnO films from similar Zn oximate complexes at  $150\text{ }^{\circ}\text{C}$  and these have been used for FET devices.<sup>70</sup> The decomposition of **2** and **3** in nitrogen follows the same trend as that of complex **1** (ESI Fig. S6<sup>†</sup>). In air, **2** and **3** undergo additional weight loss at

higher temperature, attributed to the removal of surface organic carbon.

#### Tin(II) oxide synthesis

SnO was synthesized by decomposing **1** and **2**, whereas **3** has not been used for the decomposition study due to its low yield during synthesis.

**SnO powder formation from 1 and 2.** **1** and **2** are heated from 140 to  $200\text{ }^{\circ}\text{C}$  for one hour in air. SnO formation is observed at  $140\text{ }^{\circ}\text{C}$  itself for **1** (Fig. 2c). The crystallinity of the formed SnO is independent of the decomposition temperature ( $140\text{--}200\text{ }^{\circ}\text{C}$ ). Amorphous SnO was obtained from **2** even at  $200\text{ }^{\circ}\text{C}$  (ESI Fig. S7<sup>†</sup>). The formation of amorphous SnO from **2** could be attributed to incomplete removal of the benzene fragment during the decomposition at  $163\text{ }^{\circ}\text{C}$ . This is supported by the appearance of signals for benzene ( $m/z\ 78$ ) and toluene ( $m/z\ 92$ ) fragments above  $400\text{ }^{\circ}\text{C}$  during the decomposition of **2** (Fig. 2b). Hence, **1** was chosen for making nanoparticles and thin films of SnO. The average crystallite size of SnO from **1** is in the range of 47–50 nm for temperatures between 140 and  $200\text{ }^{\circ}\text{C}$ , determined by using the Scherrer equation. Raman spectra of SnO from **1** recorded from 100 to  $500\text{ cm}^{-1}$  show



**Scheme 2** Proposed decomposition of **1** and **2** based on TG-IR and TG-MS measurements.

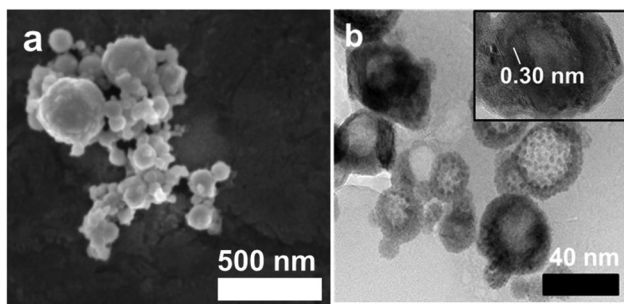


Fig. 3 (a) SEM and (b) TEM images of SnO from the decomposition of **1** at 200 °C. Spherical particles observed at 200 °C and composed of smaller particles of 10 nm grouped together as well as forming hollow spheres. Inset: atomic fringes of the 101 plane of SnO.

two vibrational absorptions at 109 and 209  $\text{cm}^{-1}$  corresponding to characteristic  $B_{1g}$  and  $A_{1g}$  modes of  $\text{SnO}^{32}$  (Fig. 2d). The similarity of the Raman spectra for both 140 °C and 200 °C shows a similar decomposition at these temperatures (ESI Fig. S8†).

Scanning and transmission electron microscopy images of SnO particles formed at 200 °C are shown in Fig. 3a and b respectively. At 200 °C SnO particles appear spherical in shape and have rough surface morphology. The particle size is between 50 and 250 nm. At 140 °C they are lumped together, with fewer non-agglomerated particles. The particle size is between 100 and 150 nm at 140 °C (ESI Fig. S9†). Transmission electron microscopy images (Fig. 3b) of the SnO particles at 200 °C indicate the presence of hollow and dense SnO particles. The high resolution TEM image (inset: Fig. 3b) shows lattice fringes of 0.30 nm spacing corresponding to the (101) plane of SnO.

Comparison of spherical SnO particles from **1** with those prepared by the aqueous route using  $\text{Sn}_6\text{O}_4(\text{OH})_4$  derived from tin halides and amides<sup>9,11,71</sup> or by vapour deposition and carbothermal reaction of  $\text{SnO}^{8,12}$  reveals various hierarchical morphologies such as nanoribbons, nanobelts, dendrimers and meshes. In addition, some level of control on the oxidation state in the final tin oxide has been achieved through the use of well-defined Sn(II) centred precursors. However, rapid precipitation in the aqueous route and formation of sub-stoichiometric tin oxide in vapour based methods are not suitable for thin film preparation. The tin oximate thus provides process flexibility for thin film preparation.

### SnO thin films from **1**

Thin films of SnO are prepared by spin-coating a saturated solution of **1** in methanol or an ethylene glycol/methanol mixture (1 : 9 v/v). The SEM micrograph of the single and 16 layers of SnO films on the Si substrate, from an ethylene glycol/methanol mixture, after heating the substrate to 200 °C is shown in Fig. 4a and b respectively. The energy-dispersive X-ray spectroscopy (EDX) analysis confirmed the presence of tin in the film for single layer SnO deposition (ESI Fig. S10†).

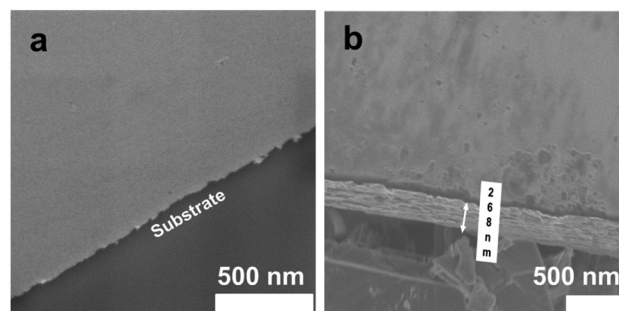


Fig. 4 SEM micrograph of SnO films (a) after one layer and (b) after 16 layers, formed by spin-coating and decomposition of **1** at 200 °C.

The 16 layer spin coated sample shows a film thickness of 268 nm. Thus, the average thickness per layer is estimated to be 16–20 nm on the silicon substrate. Comparison of the morphology of SnO thin films from reported metalorganic precursors<sup>31,32,34</sup> showed platelets and cubes with several grain boundaries, whereas with **1**, smooth films could be obtained over a larger area.

UV-Vis spectra of the SnO film recorded in the diffuse reflection setup show a band gap in the range of 3.0–3.3 eV (ESI Fig. S11†) and are comparable to the reported data.<sup>72</sup> X-ray photoelectron spectroscopy (XPS) spectra for the samples spin coated with 10 layers of SnO are shown in Fig. S12a–c (ESI†). The XPS survey spectrum of the SnO layer indicates incorporation of carbon and a small amount of nitrogen (ESI, Fig. S13 and S14†). The occlusion of these elements could be due to the residual solvent remaining or the incomplete removal of the decomposition product of **1** during several heating cycles. The binding energies of 487.0 and 495.4 eV can be assigned to Sn  $3d_{5/2}$  and  $3d_{3/2}$  electrons of tin<sup>28</sup> (Fig. S12a, ESI†). The O1s spectral line shows binding energies of 530.8 eV and 532.4 eV. The binding energy of 530.8 eV can be correlated to lattice oxygen in the tin oxide film and 532.4 eV for adsorbed OH on the surface<sup>73</sup> (Fig. S12b, ESI†). The valence band spectral peaks at 9 eV and below 2 eV (ref. 32 and 74) due to the formation of antibonding and bonding Sn(II) 5s–O 2p states were not observed, indicating that the surface of the SnO film from **1** has oxidised to Sn(IV) (Fig. S12c, ESI†). Thus it can be concluded that the SnO film reacts with adsorbed/atmospheric oxygen to convert to  $\text{SnO}_2$  as observed in the XPS analysis. A similar surface oxidation was observed for the SnO film deposited from Sn(II) bis(ureide) during its exposure to an ambient atmosphere.<sup>32</sup>

To understand the oxidation of the deposited SnO thin film, a drop-cast film from **1** in DMF solution on the Si substrate is analysed by IR before heating and by Raman spectroscopy after heating to 200 °C. IR spectra of the precursor film on Si and **1** as powder show the same absorption bands (ESI, Fig. S15†), indicating that **1** remains in the Sn(II) state on the substrate. Raman spectra of the SnO film formed after heating to 200 °C show both the characteristic  $B_{1g}$  and  $A_{1g}$  vibrational modes (Fig. 2d), in agreement with the SnO powder

produced from **1** at 200 °C. This result clearly indicates that the observed Sn(IV) state in the XPS analysis is due to the surface oxidation.

The SnO thin films formed from the reported metalorganic precursor *e.g.* Sn<sub>6</sub>O<sub>4</sub>(OSiMe<sub>3</sub>)<sub>4</sub>, [Sn(OSiMe<sub>3</sub>)<sub>2</sub>]<sub>2</sub>, Sn(II)bis-(ureide) (ureide = *t*-BuNCONMe<sub>2</sub>), and [Sn(μ-ONep)]<sub>2</sub>∞ (ONep = OCH<sub>2</sub>CMe<sub>3</sub>)<sup>31,32,34</sup> indicate stringent control of the oxygen environment, higher deposition temperature (>300 °C) and formation of metallic Sn along with the desired tin(II) oxide phase. The air/moisture sensitivity of these precursors and the disproportionation of SnO to Sn and SnO<sub>2</sub> at higher temperature make the process complicated. The air/moisture stability, low decomposition temperature and solubility of **1** in common organic solvents make it suitable for large area processing such as spin coating and printing.

Thin films of SnO of thickness 30–50 nm and 300–400 nm were prepared on the interdigitated substrate at 200 °C. The *I*-*V* characteristics of these films in the forward bias indicate the semiconducting properties of the film (ESI Fig. S16 and S17†) with a breakdown voltage of 8.9 V in the forward bias. Further studies to understand the thin film behaviour for transistor applications are currently underway.

## Conclusions

Tin(II) ketoacidoximate complexes were successfully synthesized and characterized. The Sn atom is four-fold coordinated and is donor stabilised by the oxime nitrogen of the ligand in all the complexes. The bis[2-(hydroxyimino)propionate] tin(II) decomposes above 140 °C in both air and nitrogen with complete elimination of the ligand to form SnO. The SnO particles of average size 50 nm were synthesized below 200 °C by heating **1**. SnO thin films of 16–20 nm thickness were prepared by spin-coating. The films slowly convert to Sn(IV) oxide at the surface on exposure to air. The bulk of the films remain in the Sn(II) state. The ambient atmosphere synthesis and processing make Sn(II) oximate attractive for solution processable applications.

## Experimental section

### Reagents and general procedures

All the syntheses were performed under an ambient atmosphere and with deionized water. SnCl<sub>2</sub>·2H<sub>2</sub>O (98%, Alfa Aesar), pyruvic acid (98%, Alfa Aesar), sodium phenyl pyruvate (98%, Sigma-Aldrich), hydroxylamine hydrochloride (99%, Sigma-Aldrich), methoxylamine hydrochloride (98%, Sigma-Aldrich), ammonium bicarbonate (≥99%, Sigma-Aldrich), methanol, ethanol and *N,N*-dimethylformamide of HPLC grade were used as-received. The melting point/decomposition of **1–3** were determined from the DTA (ESI Fig. S18†).

### Precursor synthesis

Syntheses of Sn ketoacidoximate complexes were performed by an adaptation of a method described previously.<sup>53,57,60</sup> The

*in situ* generation of the α-ketoacid oxime ligand in water was carried out according to the procedure described by Spenser *et al.*<sup>40</sup>

**Synthesis of bis[2-(hydroxyimino)propionate] tin(II) (1).** Ammonium bicarbonate (9.49 g, 120 mmol) was added portionwise to a stirred solution of hydroxylamine hydrochloride (4.17 g, 60 mmol) and pyruvic acid (5.28 g, 60 mmol) in water (50 mL) at room temperature and the mixture was stirred until all gas evolution had ceased. SnCl<sub>2</sub>·2H<sub>2</sub>O (6.77 g, 30 mmol) was then added, and the mixture was stirred for 4 h, after which a white powder of **1** was filtered off and washed with ice cold water. The single crystals were obtained from concentrated ethanol solution of the compound at –35 °C. Yield (6.5 g, 67%), mp 161 °C (TG) (decomp.), Found: C, 22.3; H, 2.5; N, 8.6, Calc. for C<sub>6</sub>H<sub>8</sub>N<sub>2</sub>O<sub>6</sub>Sn: C, 22.3; H, 2.5; N, 8.7%, IR (ν<sub>max</sub>/cm<sup>-1</sup>) ATR, powder: 3170 (w), 3050 (w), 2797 (w), 2725 (w), 1584 (s), 1487 (ms), 1366 (s), 1345 (s), 1195 (s), 1049 (s), 851(s), 759 (ms), 732 (s), <sup>1</sup>H NMR (400 MHz; (CD<sub>3</sub>)<sub>2</sub>SO, 25 °C), δ: 1.95 (s, 6H, CH<sub>3</sub>-C=N), <sup>13</sup>C NMR (100 MHz; (CD<sub>3</sub>)<sub>2</sub>SO, 25 °C) δ: 11.5 (CH<sub>3</sub>-C=N), 151.1 (C=N), 167.2 (C=O).

**Synthesis of bis[2-(hydroxyimino)3-phenyl-propionate] tin(II) (2).** Ammonium bicarbonate (0.395 g, 5 mmol) was added portionwise to a solution of hydroxylamine hydrochloride (0.347 g, 5 mmol) in 10 mL water and the mixture was stirred until all gas evolution had ceased. To the above solution sodium phenyl pyruvate (0.931 g, 5 mmol) in water (10 mL) was added at room temperature. The reaction was allowed to continue for 2 h. To the above mixture SnCl<sub>2</sub>·2H<sub>2</sub>O (0.564 g, 2.5 mmol) was then added, and the mixture was stirred for 4 h, after which a creamy yellow powder **2** was filtered off and washed with ice cold water. The single crystals were obtained from concentrated methanol solution by the slow evaporation method. Yield (1 g, 78%), mp 163 °C (TG) (decomp.), Found C, 44.1; H, 3.4; N, 6.1, Calc. for C<sub>18</sub>H<sub>16</sub>N<sub>2</sub>O<sub>6</sub>Sn: C, 45.5; H, 3.4; N, 5.9%, IR (ν<sub>max</sub>/cm<sup>-1</sup>) ATR, powder: 3175 (w), 3062 (w), 2846 (w), 1600 (s), 1493 (m), 1453 (w), 1426 (w), 1373 (ms), 1337 (w), 1298 (w), 1230 (ms), 1158 (ms), 1137 (ms), 1055 (s), 1026 (s), 931 (w), 862 (s), 774 (ms), 754 (m), 715 (s), 695 (s), 552 (w), <sup>1</sup>H NMR (400 MHz; (CD<sub>3</sub>)<sub>2</sub>SO, 25 °C), δ: 3.83 (s, 4H, -CH<sub>2</sub>-Ph), 7.24 (s, 10H, Ph) 12.4 (s, 2H, -N-OH), <sup>13</sup>C NMR (100 MHz; (CD<sub>3</sub>)<sub>2</sub>SO, 25 °C) δ: 30.7(-CH<sub>2</sub>), 126.6 (Ph), 128.7 (Ph), 129.2 (Ph), 137.1(Ph) 152.2 (C=N), 167.1 (C=O).

**Synthesis of diaqua tris[2-(methoxyimino)propionate] tin(II) ammonium salt (3).** Ammonium bicarbonate (9.49 g, 120 mmol) was added portionwise to a stirred solution of methoxylamine hydrochloride (5.01 g, 60 mmol) and pyruvic acid (5.28 g, 60 mmol) in water (30 mL) at room temperature, and the mixture was stirred until all gas evolution had ceased and was stirred further for 3 h. SnCl<sub>2</sub>·2H<sub>2</sub>O (6.77 g, 30 mmol) was then added; at the start, the reaction is slow. As time progresses a white precipitate is seen. The precipitate is dissolved in ethanol, reduced in volume and kept at –35 °C for recrystallization. Yield (0.8 g, 10%), mp 151 °C (TG) (decomp.), Found C: 27.9, H: 4.2, N: 10.3, Calc. for C<sub>12</sub>H<sub>26</sub>N<sub>4</sub>O<sub>11</sub>Sn: Calc. C: 27.7, H: 5.0, N: 10.8%. IR (ν<sub>max</sub>/cm<sup>-1</sup>) ATR, powder: 3284 (w), 3144 (w), 3052 (w), 2988 (w), 2943 (w), 2827 (w) 1649 (ms),

1633 (s), 1593(s), 1536 (m), 1442 (m), 1418 (ms), 1371 (w), 1349 (s), 1204(s), 1172 (s), 1043, (s) 927 (ms), 855 (s), 768 (m), 723 (s), 579(m), <sup>1</sup>H NMR (400 MHz; (CD<sub>3</sub>)<sub>2</sub>SO, 25 °C), δ: 1.91 (s, 9H, N=C-CH<sub>3</sub>), 3.93 (s, 9H, N-OCH<sub>3</sub>), <sup>13</sup>C NMR (100 MHz; (CD<sub>3</sub>)<sub>2</sub>SO, 25 °C) δ: 12.3(N=C-CH<sub>3</sub>), 62.4(N-OCH<sub>3</sub>), 152.7 (C=N), 168.0 (C=O).

### Synthesis of SnO

**Heating 1.** 150 mg of complex **1** is heated in a nickel crucible to 140–200 °C in air for one hour in a general purpose laboratory furnace. 52 mg (83 % yield based on Sn supplied in 150 mg of complex **1**).

**Thin film deposition – spin coating.** A saturated solution of **1** in methanol or ethylene glycol mixture (9 : 1) is used to spin-coat a thin layer of precursor on the Si substrate. A filtered, 50 μL of the solution is dropped on the substrate with the coating programme of 1000 rpm/30 seconds/5000 rpm/20 seconds. The relative humidity during spin coating was between 57 and 60%.

**Thin film deposition – drop casting.** 100 μL of a saturated solution of **1** in DMF is drop-cast on the Si substrate. The solvent is allowed to evaporate in a well-ventilated chemical hood.

### Characterization

IR spectroscopic measurements were carried out using a Nicolet iS10 FTIR spectrometer with the ATR setup. The scans were performed from 4000 to 525 cm<sup>-1</sup>. <sup>1</sup>H NMR and <sup>13</sup>C NMR spectra were recorded on a Bruker AC300F spectrometer at 400 MHz. Elemental analysis (C,H,N) was performed on a Flash 2000 instrument from Thermo Scientific. Thermogravimetry measurements were carried out using a Netzsch STA 449 F3 Jupiter instrument equipped with a TG/DSC sample carrier. Thermogravimetry coupled infrared (TG-IR) measurements were performed on a Netzsch TGA 289 F1 Iris instrument coupled to a Tensor 27 TGA-IR. Thermogravimetry coupled mass spectrometry (TG-MS) measurements were carried out on a Netzsch TG 209 F1 Iris coupled with a QMS 403 C Aelos mass spectrometer. Micro Raman measurements were performed on a LabRAM HR high resolution microscope from Horiba Jobin Yvon (model HR 800). The excitation wavelength was 532.2 nm. The spectrum was recorded in the range of 50–1000 cm<sup>-1</sup>. X-ray powder diffraction patterns (XRD) of the samples at room temperature were recorded using a STOE Stadi MP instrument equipped with a Cu-Kα<sub>1</sub> source and a Mythen detector. SEM investigations were performed with a Quanta 600 FEG microscope typically at low keV (3–5 keV). TEM analysis was conducted on a Titan Super Twin instrument at 300 kV.

Single-crystal X-ray diffraction experiments for **1–3** were carried out on an IPDS2 (STOE) image plate diffractometer with graphite monochromatized Mo-Kα (λ = 0.71069 Å) radiation, at 150 K with a detector distance of 100 mm. Single crystals of **1–3** were mounted on a glass capillary using perfluoroalkylether (viscosity 1800 cSt., ABCR GmbH & Co. KG, Karlsruhe). For data collection, determination, and refinement

of the lattice parameters as well as for data reduction including LP correction, the STOE X-Area<sup>75</sup> software package was used. The intensity data were corrected for absorption numerically using the crystal habit and the program X-Shape.<sup>76</sup> The crystal structure was solved by direct methods and refined using the program packages SHELXS97 and SHELXL97.<sup>77</sup>

## Acknowledgements

This work was supported by the King Abdullah University of Science & Technology (KAUST) baseline (BAS/1/1302-01-01) and AEA funding. J. K. thanks Dr Rachid Sougrat and Ms Nini Wei for TEM imaging and Dr Mohamed Nejib Hedhili for XPS analysis.

## Notes and references

- 1 P. P. Edwards, A. Porch, M. O. Jones, D. V. Morgan and R. M. Perks, *Dalton Trans.*, 2004, 2995–3002.
- 2 B. G. Lewis and D. C. Paine, *MRS Bull.*, 2000, 25, 22–27.
- 3 E. N. Dattoli, Q. Wan, W. Guo, Y. Chen, X. Pan and W. Lu, *Nano Lett.*, 2007, 7, 2463–2469.
- 4 C. W. Ou, Dhananjay, Z. Y. Ho, Y. C. Chuang, S. S. Cheng, M. C. Wu, K. C. Ho and C. W. Chu, *Appl. Phys. Lett.*, 2008, 92, 122113.
- 5 M. Batzill and U. Diebold, *Prog. Surf. Sci.*, 2005, 79, 47.
- 6 J. R. Brown, M. T. Cheney, P. W. Haycock, D. J. Houlton, A. C. Jones and E. W. Williams, *J. Electrochem. Soc.*, 1997, 144, 295–299.
- 7 G. Frank, E. Kauer, H. Köstlin and F. J. Schmitte, *Sol. Energy Mater.*, 1983, 8, 387–398.
- 8 B. Kumar, D. H. Lee, S. H. Kim, B. Yang, S. Maeng and S.-W. Kim, *J. Phys. Chem. C*, 2010, 114, 11050–11055.
- 9 H. Uchiyama and H. Imai, *Langmuir*, 2008, 24, 9038–9042.
- 10 Z. L. Wang and Z. W. Pan, *Adv. Mater.*, 2002, 14, 1029–1032.
- 11 H. Uchiyama and H. Imai, *Cryst. Growth Des.*, 2007, 7, 841–843.
- 12 M. O. Orlandi, E. R. Leite, R. Aguiar, J. Bettini and E. Longo, *J. Phys. Chem. B*, 2006, 110, 6621–6625.
- 13 D. Aurbach, A. Nimberger, B. Markovsky, E. Levi, E. Sominski and A. Gedanken, *Chem. Mater.*, 2002, 14, 4155–4163.
- 14 N. Xiao, C. Li, D. Li, B. Liu, B. Zou, G. Zou, W. W. Yu, J. Ning, Q. Dai, T. Jiang, K. Men and D. Liu, *Langmuir*, 2009, 25, 1818–1821.
- 15 H. Giefersa, F. Porsch and G. Wortmanna, *Solid State Ionics*, 2005, 176, 199–207.
- 16 Y. He, D. Li, J. Chen, Y. Shao, J. Xian, X. Zheng and P. Wang, *RSC Adv.*, 2014, 4, 1266–1269.
- 17 Z. R. Dai, Z. W. Pan and Z. L. Wang, *J. Am. Chem. Soc.*, 2002, 124, 8673–8680.

- 18 H. Wang, Y. Wang, J. Xu, H. Yang, C.-S. Lee and A. L. Rogach, *Langmuir*, 2012, **28**, 10597–10601.
- 19 Y. Ogo, H. Hiramatsu, K. Nomura, H. Yanagi, T. Kamiya, M. Hirano and H. Hosono, *Appl. Phys. Lett.*, 2008, **93**, 032113.
- 20 H. Hosono, Y. Ogo, H. Yanagi and T. Kamiya, *Electrochem. Solid-State Lett.*, 2011, **14**, H13–H16.
- 21 K. Nomura, T. Kamiya and H. Hosono, *Adv. Mater.*, 2011, **23**, 3431–3434.
- 22 J. Um and S. E. Kim, *ECS Solid State Lett.*, 2014, **3**, P94–P98.
- 23 L. Liang and H. Cao, *ECS Trans.*, 2013, **50**, 289–297.
- 24 I. C. Chiu and I. C. Cheng, *IEEE Electron Device Lett.*, 2014, **35**, 90–92.
- 25 P.-C. Hsu, W.-C. Chen, Y.-T. Tsai, Y.-C. Kung, C.-H. Chang, C.-J. Hsu, C.-C. Wu and H.-H. Hsieh, *Jpn. J. Appl. Phys.*, 2013, **52**, 05DC07.
- 26 L. Y. Liang, Z. M. Liu, H. T. Cao, W. Y. Xu, X. L. Sun, H. Luo and K. Cang, *J. Phys. D: Appl. Phys.*, 2012, **45**, 085101.
- 27 H. Yabuta, N. Kaji, R. Hayashi, H. Kumomi, K. Nomura, T. Kamiya, M. Hirano and H. Hosono, *Appl. Phys. Lett.*, 2010, **97**, 072111.
- 28 A. C. Saritha, K. S. Sasanka, M. Majeesh, K. Hasna, P. P. Subha, L. S. Vikas and M. K. Jayaraj, *J. Electr. Devices*, 2014, **19**, 1642–1647.
- 29 H. Luo, L. Y. Liang, H. T. Cao, Z. M. Liu and F. Zhuge, *ACS Appl. Mater. Interfaces*, 2012, **4**, 5673–5677.
- 30 T. Toyama, Y. Seo, T. Konishi, H. Okamoto and Y. Tsutsumi, *Appl. Phys. Express*, 2011, **4**, 071101.
- 31 I. Barbul, A. L. Johnson, G. Kociok-Köhn, K. C. Molloy, C. Silvestru and A. L. Sudlow, *ChemPlusChem*, 2013, **78**, 866–874.
- 32 T. Wildsmith, M. S. Hill, A. L. Johnson, A. J. Kingsley and K. C. Molloy, *Chem. Commun.*, 2013, **49**, 8773–8775.
- 33 J. H. Han, Y. J. Chung, B. K. Park, S. K. Kim, H.-S. Kim, C. G. Kim and T.-M. Chung, *Chem. Mater.*, 2014, **26**, 6088–6091.
- 34 T. J. Boyle, T. L. Ward, S. M. De'Angeli, H. Xu and W. F. Hammetter, *Chem. Mater.*, 2003, **15**, 765–775.
- 35 K. Okamura, B. Nasr, R. A. Brand and H. Hahn, *J. Mater. Chem.*, 2012, **22**, 4607–4610.
- 36 X. Q. Pan and L. Fu, *J. Appl. Phys.*, 2001, **89**, 6048–6055.
- 37 W. K. Choi, H. Sung, K. H. Kim, J. S. Cho, S. C. Choi, H. J. Jung, S. K. Koh, C. M. Lee and K. Jeong, *J. Mater. Sci. Lett.*, 1997, **16**, 1551–1554.
- 38 V. Y. Kukushkin and A. J. L. Pombeiro, *Coord. Chem. Rev.*, 1999, **181**, 147–175.
- 39 N. Gerasimchuk, *Eur. J. Inorg. Chem.*, 2014, 4518–4531, DOI: 10.1002/ejic.201402251.
- 40 A. Ahmad and I. D. Spenser, *Can. J. Chem.*, 1961, **39**, 1340–1359.
- 41 J. J. Schneider, R. C. Hoffmann, J. Engstler, S. Dilfer, A. Klyszcz, E. Erdem, P. Jakes and R. A. Eichel, *J. Mater. Chem.*, 2009, **19**, 1449–1457.
- 42 N. Gerasimchuk, T. Maher, P. Durham, K. V. Domasevitch, J. Wilking and A. Mokhir, *Inorg. Chem.*, 2007, **46**, 7268–7284.
- 43 A. Szorcsik, L. Nagy, L. Pellerito and R. D. Lampeka, *J. Radioanal. Nucl. Chem.*, 2003, **257**, 285–291.
- 44 R. Lampeka, R. Bergs, R. Krämer, K. Polborn and K. Beck, *Z. Naturforsch., B: Chem. Sci.*, 1994, **49**, 225–232.
- 45 R. Krämer, H. Wanjek, K. Polborn and W. Beck, *Chem. Ber.*, 1993, **126**, 2421–2427.
- 46 T. Y. Sliva, R. D. Lampeka, G. V. Vladyko, E. I. Boreko and L. V. Korobchenko, *Pharm. Chem. J.*, 1992, **26**, 613–615.
- 47 A. W. Apblett and G. D. Georgieva, *Phosphorus, Sulfur Silicon Relat. Elem.*, 2009, **93**, 479–480.
- 48 R. D. Lampeka, N. M. Dudarenko and V. V. Skopenko, *Acta Crystallogr., Sect. C: Cryst. Struct. Commun.*, 1994, **50**, 706–708.
- 49 M. V. Kirillova, M. Haukka, A. M. Kirillov, J. A. L. Silva, J. J. R. Frausto da Silva and A. J. L. Pombeiro, *Acta Crystallogr., Sect. E: Struct. Rep. Online*, 2007, **63**, m1670–m1671.
- 50 I. Georgieva, N. Trendafilova and G. Bauer, *Spectrochim. Acta, Part A*, 2006, **63**, 403–415.
- 51 R. D. Lampeka, Z. D. Uzakbergenova and V. V. Skopenko, *Z. Naturforsch., B: Chem. Sci.*, 1993, **48**, 409–417.
- 52 A. Kufelnicki, S. V. Tomy, V. Vitske, J. Jaciubek-Rosińska, M. Haukka and I. O. Fritsky, *Polyhedron*, 2013, **56**, 144–151.
- 53 M. R. Hill, A. W. Jones, J. J. Russell, N. K. Roberts and R. N. Lamb, *Inorg. Chim. Acta*, 2005, **358**, 201–206.
- 54 A. W. Apblett, G. D. Georgieva and J. T. Mague, *Inorg. Chem.*, 1997, **36**, 2656–2661.
- 55 A. W. Apblett, G. D. Georgieva and J. T. Mague, *Can. J. Chem.*, 1997, **75**, 483–490.
- 56 K. Malek, M. Vala, J. Swiatek-Kozłowska and L. M. Proniewicz, *New J. Chem.*, 2004, **28**, 477–483.
- 57 Z. Zhang, R. Liu, M. Zhao and Y. Qian, *Mater. Chem. Phys.*, 2001, **71**, 161–164.
- 58 Y. S. Wang, P. J. Thomas and P. O'Brien, *J. Phys. Chem. B*, 2006, **110**, 4099–4104.
- 59 Y. S. Wang, *J. Cryst. Growth*, 2006, **291**, 398–404.
- 60 J. Khanderi, C. Contiu, J. Engstler, R. C. Hoffmann, J. J. Schneider, A. Drochner and H. Vogel, *Nanoscale*, 2011, **3**, 1102–1112.
- 61 M. Pashchanka, R. C. Hoffmann and J. J. Schneider, *J. Mater. Chem.*, 2010, **20**, 957–963.
- 62 C. Pettinari, F. Marchetti, R. Pettinari, A. Cingolani, E. Rivarola, C. Phillips, J. Tanski, M. Rossi and F. Caruso, *Eur. J. Inorg. Chem.*, 2004, **2004**, 3484–3497.
- 63 A. W. Addison, T. N. Rao, J. Reedijk, J. van Rijn and G. C. Verschoor, *J. Chem. Soc., Dalton Trans.*, 1984, 1349–1356.
- 64 L. Iovkova-Berends, T. Berends, T. Zöllner, G. Bradtmöller, S. Herres-Pawlis and K. Jurkschat, *Eur. J. Inorg. Chem.*, 2012, **2012**, 3191–3199.
- 65 L. Iovkova-Berends, T. Berends, T. Zöllner, D. Schollmeyer, G. Bradtmöller and K. Jurkschat, *Eur. J. Inorg. Chem.*, 2012, **2012**, 3463–3473.
- 66 T. Berends, L. Iovkova, G. Bradtmöller, I. Opiel, M. Schürmann and K. Jurkschat, *Z. Anorg. Allg. Chem.*, 2009, **635**, 369–374.
- 67 L. Gracia, A. Beltrán and J. Andrés, *J. Phys. Chem. B*, 2007, **111**, 6479–6485.

- 68 D. Le Bellac, J. M. Kiat, P. Garnier, H. Moudden, P. Sciau, P. A. Buffat and G. André, *Phys. Rev. B: Condens. Matter*, 1995, **52**, 13184–13194.
- 69 E. Hennings, H. Schmidt, M. Kohler and W. Voigt, *Acta Crystallogr., Sect. E: Struct. Rep. Online*, 2014, **70**, 474–476.
- 70 J. J. Schneider, R. C. Hoffmann, J. Engstler, O. Soffke, W. Jaegermann, A. Issanin and A. Klyszcz, *Adv. Mater.*, 2008, **20**, 3383–3387.
- 71 J. Khanderi, L. Shi and A. Rothenberger, *Inorg. Chim. Acta*, 2015, **427**, 27–32.
- 72 W. Guo, L. Fu, Y. Zhang, K. Zhang, L. Y. Liang, Z. M. Liu, H. T. Cao and X. Q. Pan, *Appl. Phys. Lett.*, 2010, **96**, 042113.
- 73 L. Yan Liang, H. Tao Cao, X. Bo Chen, Z. Min Liu, F. Zhuge, H. Luo, J. Li, Y. Cheng Lu and W. Lu, *Appl. Phys. Lett.*, 2012, **100**, 263502.
- 74 L. Kover, Z. Kovacs, R. Sanjines, G. Moretti, I. Cserny, G. Margaritondo, J. Palinkas and H. Adachi, *Surf. Interface Anal.*, 1995, **23**, 461–466.
- 75 X-Area, *STOE's Area Detector Software and IPDS software*, STOE & Cie., Darmstadt, 2006.
- 76 X-Shape, *Crystal Optimisation for Numerical Absorption Correction*, STOE & Cie., Darmstadt, 1999.
- 77 G. M. Sheldrick, *SHELX97, Programs for the Solution and Refinement of Crystal Structures*, University of Goettingen, Germany, 1997.